Core crystallization and pile-up in the cooling sequence of evolving white dwarfs

Pier-Emmanuel Tremblay[1]*, Gilles Fontaine[2], Nicola Pietro Gentile Fusillo[1], Bart H. Dunlap[3], Boris T. Gänsicke[1], Mark A. Hollands[1], J. J. Hermes[3], Thomas R. Marsh[1], Elena Cukanovaite[1] & Tim Cunningham[1]

White dwarfs are stellar embers depleted of nuclear energy sources that cool over billions of years[1]. These stars, which are supported by electron degeneracy pressure, reach densities of 10^7 grams per cubic centimetre in their cores[2]. It has been predicted that a first-order phase transition occurs during white-dwarf cooling, leading to the crystallization of the non-degenerate carbon and oxygen ions in the core, which releases a considerable amount of latent heat and delays the cooling process by about one billion years[3]. However, no direct observational evidence of this effect has been reported so far. Here we report the presence of a pile-up in the cooling sequence of evolving white dwarfs within 100 parsecs of the Sun, determined using photometry and parallax data from the Gaia satellite[4]. Using modelling, we infer that this pile-up arises from the release of latent heat as the cores of the white dwarfs crystallize. In addition to the release of latent heat, we find strong evidence that cooling is further slowed by the liberation of gravitational energy from element sedimentation in the crystallizing cores[5–7]. Our results describe the energy released by crystallization in strongly coupled Coulomb plasmas[8,9], and the measured cooling delays could help to improve the accuracy of methods used to determine the age of stellar populations from white dwarfs[10].

The white-dwarf cooling age at which crystallization sets in has been predicted to depend on the mass (Fig. 1), with more massive white dwarfs entering this phase transition earlier[3]. Another major event in the evolution of a white dwarf is the direct coupling between its degenerate core and convective envelope[11], which results in an initial decrease in cooling rates followed by an increase. At the low white-dwarf masses (about $0.55M_\odot$, where $M_\odot$ is the mass of the Sun) of old stellar populations in globular clusters, this event occurs at a similar age as crystallization but has a stronger signature[12]. Previous attempts to measure cooling effects from crystallization in clusters have therefore provided indirect evidence based on linking the white-dwarf and main-sequence turn-off age determinations[13]. By contrast, crystallization occurs much earlier than convective coupling in white dwarfs more massive than $0.7M_\odot$. The observational implication of this prediction, reported over fifty years ago[3], is an isolated crystallization sequence in the Hertzsprung–Russell (colour $G_{\rm PB} - G_{\rm RP}$ versus absolute magnitude $G_{\rm abs}$) diagram, yet no direct observational evidence of this effect existed until now.

Because of their small radii, typically of the order of $0.01R_\odot$ ($R_\odot$ is the radius of the Sun), white dwarfs are intrinsically faint; consequently, until recently very few had accurate distance measurements, which are needed to determine their luminosities[14]. The second data release of the European Space Agency Gaia mission[4] (Gaia DR2) has led to a breakthrough, defining the first empirical cooling sequence of field white dwarfs in the Hertzsprung–Russell diagram[15]. Although previous studies have investigated the cooling sequences of white dwarfs in old globular clusters[16], only a local volume-limited sample can contain white dwarfs spanning the full ranges of total age and initial mass[17].

We use a recently established catalogue of high-confidence Gaia white-dwarf candidates[18] to extract degenerate stars within 100 pc of the Sun. The selection function of Gaia is found to be colour- and magnitude-independent down to the sky-position-dependent faint-magnitude limit[18], and the Gaia median parallax precision of 1.5% allows unambiguous transformation to distances. For 15,109 sources the Gaia photometric and astrometric data are reliable enough

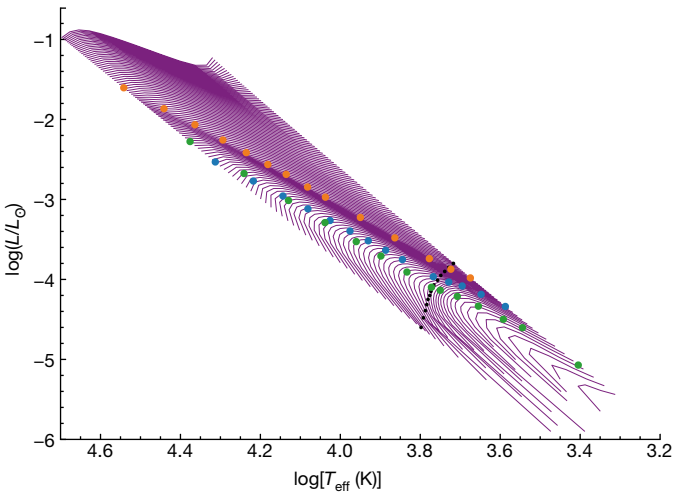

Fig. 1 | Effects of crystallization on the cooling of white dwarfs. The closely spaced isochrones in effective-temperature–luminosity ($T_{\rm eff}$–L) space connect white dwarfs of the same age but with different masses. The cooling age is $\log[t_{\rm cool}\ ({\rm yr})] = 7.5$ at the top, with subsequent increments of $\Delta\log[t_{\rm cool}\ ({\rm yr})] = 0.02$, and the mass varies from $0.4M_\odot$ on the low-$T_{\rm eff}$ sides of the isochrones to $1.3M_\odot$ on the high-$T_{\rm eff}$ sides. The (variable) density of these isochrones illustrates phases of slowing and accelerated cooling. All models used to obtain these results consider standard pure-hydrogen-atmosphere DA white dwarfs with the same envelope stratification ($M_{\rm H}/M_{\rm wd} = 10^{-4}$ and $M_{\rm He}/M_{\rm wd} = 10^{-2}$) and core composition (^{12}C and ^{16}O in equal mass proportions and distributed homogeneously)[11]. The models include the release of latent heat, but no additional energy source associated with phase separation[5–7]. The orange dots indicate the onset of crystallization at the centre of the evolving model in selected evolutionary sequences. At that point, as the crystallization front progresses upwards in the star from the centre, latent heat is liberated, forming a crest of isochrones that form a 'transverse' sequence. Because the internal energy is discontinuous between the liquid and solid phases, this predicted phase transition is of the first order[3]. The blue dots indicate locations where 80% of the mass has solidified. Following this event, the most remarkable effect of crystallization on the cooling of white dwarfs is the so-called Debye cooling phase[6,11], that is, the transition from the classical regime to the quantum regime (green dots) in the solid state. Finally, the onset of the coupling between the upper convection zone with the degenerate core[25] is illustrated by the black dots.

[1]Department of Physics, University of Warwick, Coventry, UK. [2]Département de Physique, Université de Montréal, Montréal, Quebec, Canada. [3]Department of Physics and Astronomy, University of North Carolina, Chapel Hill, NC, USA. *e-mail: p-e.tremblay@warwick.ac.uk

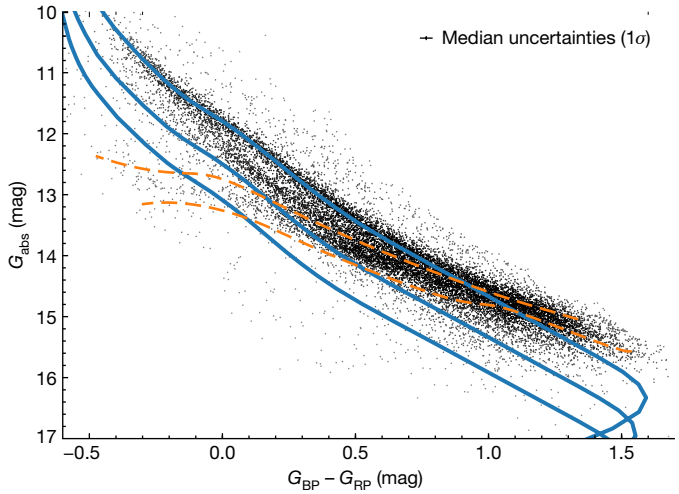

Fig. 2 | Observational Gaia colour–magnitude Hertzsprung–Russell diagram for white dwarfs within 100 pc of the Sun. Dereddened G, G_{BP} and G_{RP} photometry and parallax results are used for 15,109 white-dwarf candidates with Gaia data reliable enough to derive atmospheric parameters[18]. For visualization purposes, the data are shown in greyscale, according to a Gaussian kernel density estimate, and with power-law scaling with an exponent of 0.25. The two orange dashed lines indicate where evolutionary models predict that 20% (top sequence) and 80% (bottom sequence) of the total white-dwarf mass has crystallized. The higher density of white dwarfs within that region corresponds to the transverse sequence discussed in the text. Three evolutionary models at $0.6M_{\odot}$, $0.9M_{\odot}$ and $1.1M_{\odot}$ (from top to bottom, blue solid lines) illustrate the evolution of hydrogen-atmosphere white dwarfs with thick hydrogen layers[11]. The bifurcation of the observed cooling sequence in two separate tracks in the range $-0.1 < G_{BP} - G_{RP} < 0.6$ and above the orange dashed curves is not caused by crystallization, but is interpreted as the different positions of hydrogen- and helium-atmosphere white dwarfs[18,20].

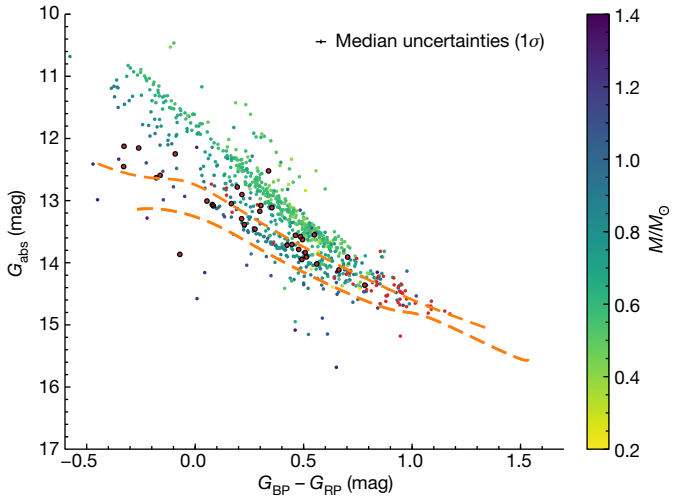

Fig. 3 | Observational Gaia Hertzsprung–Russell diagram for white dwarfs with SDSS spectra. Included are 798 objects within 100 pc of the Sun that show the presence of hydrogen Balmer lines and no helium lines or red excess from a companion[18]. White dwarfs are colour-coded (see colour scale) according to their independently determined spectroscopic masses[19,22,23] except when lines are too weak to derive masses ($\sigma_m/M > 50\%$, where σ_m is the median uncertainty; red dots) or there is evidence of a magnetic field (>2 MG) from Zeeman line splitting (red dots with black outlines). The two orange dashed lines indicate where evolutionary models predict that 20% (top) and 80% (bottom) of the total white-dwarf mass has solidified. This region, where the bulk of the crystallization occurs, shows an overdensity of objects.

to provide the surface temperature, surface gravity and mass[18] by fitting the data with model atmospheres[19] and standard evolutionary tracks with $^{12}C/^{16}O$ core composition and thick H envelopes[11]. Sloan Digital Sky Survey (SDSS) spectroscopic data are available for 1,309 of the white dwarfs within 100 pc of the Sun, providing their atmospheric composition.

The 100-pc field white-dwarf cooling sequence exhibits a substantial amount of structure (Fig. 2). The bifurcation into two sub-sequences in the range $-0.1 < G_{BP} - G_{RP} < 0.6$ has been shown to be a split between H atmospheres in the upper branch and helium-dominated atmospheres in the lower branch[18,20]. These two branches correspond to cooling tracks at the median (about $0.6M_{\odot}$) white-dwarf mass. More massive white dwarfs have larger absolute magnitudes because of their mass–radius relation[21] and are therefore expected to populate the area below the principal branches. A third, separate 'transverse' sequence is visible at lower absolute magnitudes. Unlike the aforementioned bifurcation, this transverse feature is inconsistent with a single-mass cooling track. This rules out a simple astrophysical explanation, such as effects from the mass loss in post-main-sequence evolution or merger products from binary evolution, as these scenarios cannot conceivably result in a tight correlation between white-dwarf mass and surface temperature that is unrelated to the cooling process.

The transverse sequence fully coincides with the range of absolute magnitudes and colours at which the bulk of the latent heat from crystallization is released for white dwarfs over the full range of masses considered. The crystallization sequence is more clearly visible when the sample is restricted to white dwarfs with more simple hydrogen-dominated atmospheres and for which independent spectroscopic parameters, determined from fitting hydrogen lines[19,22,23], agree with their position in the Hertzsprung–Russell diagram (Fig. 3). Roughly 8% of sources within the crystallized sequence harbour large (>2 MG) global magnetic fields, detected from Zeeman splitting[18]. Helium-atmosphere white dwarfs also populate the cooler and less massive ($<0.7M_{\odot}$) area of the sequence. There is a dearth of massive helium-atmosphere stellar remnants in all parts of the Hertzsprung–Russell diagram, including the crystallized sequence, which is probably caused by single-star evolution not forming thin hydrogen layers for higher mass progenitors[24]. The 100-pc sample was cross-matched with the Galex, 2MASS, WISE, Pan-STARRS and SDSS photometric datasets, and it was determined that white dwarfs within the transverse sequence are underluminous at all wavelengths compared to objects in the dominant cooling sequence; therefore, they behave as genuine high-mass objects. We conclude that nothing stands out in the atmospheric properties of the white dwarfs in the crystallized sequence, apart from a tight correlation between colour and absolute magnitude. An explanation consistent with these results is crystallization, a cooling effect that is expected to impact white dwarfs of similar mass and interior composition at the same age, with little influence from their atmospheric composition or the presence of magnetic fields[2,25].

The crystallized sequence is not a cooling track but a mass-dependent pile-up across the Hertzsprung–Russell diagram resulting from the white dwarfs spending more time at this location as they release their latent heat. To further characterize this process we extracted the white-dwarf luminosity function in the mass range $(0.9–1.1)M_{\odot}$ from the Gaia 100-pc sample (Fig. 4). Two peaks are clearly seen in the luminosity function: one at higher luminosities, which is attributed to crystallization, and the other one at lower luminosities, which is unambiguously linked to the finite age of the Galactic disk[10]. At masses lower than those considered here, crystallization occurs at fainter absolute magnitudes, where it overlaps both with the convective coupling of the core with the envelope and the peak in the luminosity function caused by the age of the Galactic disk.

We performed white-dwarf population simulations (Fig. 4) assuming constant stellar formation over the past 10 Gyr, the Salpeter initial-mass function, a standard initial-to-final-mass relation[26] coupled with predicted main-sequence lifetimes[27], and a Gaia magnitude limit of $G = 20$. These input parameters do not influence the slope of the luminosity function where crystallization occurs, so we made no

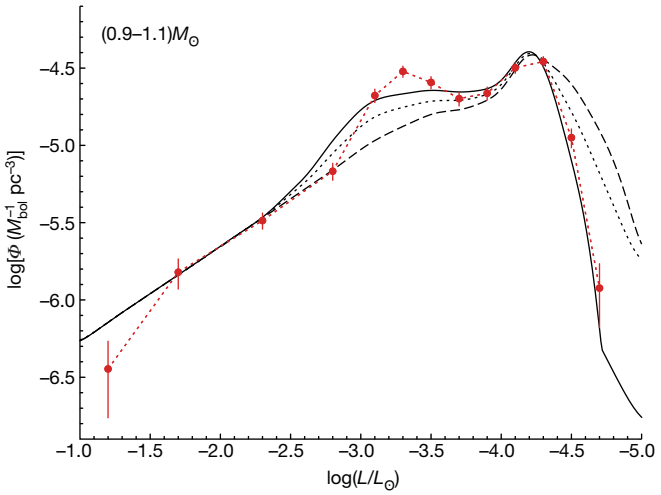

Fig. 4 | Luminosity function for massive white dwarfs within 100 pc of the Sun. Stellar remnants with Gaia-derived masses between $0.9M_\odot$ and $1.1M_\odot$ are used to calculate the observed luminosity function Φ (connected red dots; M_{bol}, bolometric absolute magnitude). Error bars are from number statistics (1σ). The first peak, on the left, is a direct observational signature of crystallization in white dwarfs. The second peak, on the right, followed by a sharp drop off at smaller luminosities, is caused by the finite age of the Galactic disk[10]. Three different predicted luminosity functions are employed to illustrate the physics of crystallization. All models use the same assumptions on Galactic evolution, including an age of 10 Gyr for the disk. In the standard case (solid line), both the latent heat released from crystallization and the gravitational energy released from ^{16}O sedimentation are included. The dotted curve neglects phase separation but includes the release of latent heat, whereas the dashed curve neglects both latent heat and phase separation. In the latter case the equation of state still transits from liquid to solid, as otherwise the solution would not be physical. The three models are arbitrarily normalized on the basis of the second- and third-highest-luminosity bins.

attempt to fit them to the observations. By contrast, the three simulations presented in Fig. 4 use different assumptions about the crystallization process, showing a strong influence on the prediction of a peak at $-3.75 < \log(L/L_\odot) < -2.75$. The case without latent heat release by crystallization is clearly ruled out by the observations. When latent heat is included in the model, there is a substantial increase in the predicted number of white dwarfs in the range of luminosity of the observed peak. The Gaia luminosity function is best reproduced when ^{16}O sedimentation is allowed to occur along with the release of latent heat. Compared with the original ^{12}C/^{16}O fluid mixture, sedimentation leaves behind a solid region that is oxygen-enriched at a level that depends on the actual composition of the fluid. The extra carbon in the fluid phase is forced upwards from a crystallizing shell, leading to a release of potential energy that further delays cooling[7]. We note that this third model, with latent heat and phase separation, provides an excellent description of the overall Gaia luminosity function, including its descending branch. The cumulative cooling delay from crystallization has a direct effect on the descending branch: stars that have higher internal energy become warmer at the same age. The model bump is not perfectly modelled, because the observed feature is narrower and of higher magnitude, but its exact shape depends on several choices, including the value of the Coulomb plasma parameter[28] ($\Gamma = 175$ here), the assumed chemical profile in the core (^{12}C and ^{16}O in equal mass proportions and distributed homogeneously), the envelope stratification ($M_H/M_{wd} = 10^{-4}$ and $M_{He}/M_{wd} = 10^{-2}$, where M_H, M_{He} and M_{wd} are the masses of hydrogen, helium and the white dwarf, respectively), as well as possible ^{22}Ne sedimentation[9,13]. More importantly, the existence and location of this bump provides strong evidence that the observed excess of white dwarfs in the Gaia transverse sequence bears the signature of crystallization.

We report direct evidence that a first-order phase transition really occurs in high-density Coulomb plasmas[3]—a theory that cannot be tested in laboratories because of the extreme densities involved—thus providing strong constraints on dense plasma physics[7–9,28]. Crystallization considerably slows the cooling process in white dwarfs. In addition, our observations require the release of gravitational energy from the separation of an initially homogeneous fluid into a stratified solid with an ^{16}O/^{12}C ratio that increases towards the centre of the star, providing a new method to test nucleosynthesis processes in low- and intermediate-mass stars[29]. The descending branch of the empirical white-dwarf luminosity function is greatly affected by phase separation[5–7] and quantum effects in Debye cooling[6,30], necessitating the understanding of these processes when relying on stellar remnants for age-dating stellar populations[10,11].

Online content

Any methods, additional references, Nature Research reporting summaries, source data, statements of data availability and associated accession codes are available at https://doi.org/10.1038/s41586-018-0791-x.

Data availability

The Gaia DR2 catalogue of white dwarfs used in this study is available from the University of Warwick astronomy catalogues repository, https://warwick.ac.uk/fac/sci/physics/research/astro/research/catalogues/gaia_dr2_white_dwarf_candidates_v2.csv. All modelling was performed with our extensive white-dwarf evolution code. We have opted not to make this multi-purpose code available, but the cooling sequences calculated for this work are available on request.

Received: 16 August 2018; Accepted: 29 October 2018;
Published online 9 January 2019.

1. Mestel, L. On the theory of white dwarf stars. I. The energy sources of white dwarfs. *Mon. Not. R. Astron. Soc.* **112**, 583–597 (1952).
2. Tassoul, M., Fontaine, G. & Winget, D. E. Evolutionary models for pulsation studies of white dwarfs. *Astrophys. J. Suppl. Ser.* **72**, 335–386 (1990).
3. van Horn, H. M. Crystallization of white dwarfs. *Astrophys. J.* **151**, 227–238 (1968).
4. Gaia Collaboration. Gaia Data Release 2. Summary of the contents and survey properties. *Astron. Astrophys.* **616**, A1 (2018).
5. Garcia-Berro, E., Hernanz, M., Mochkovitch, R. & Isern, J. Theoretical white-dwarf luminosity functions for two phase diagrams of the carbon-oxygen dense plasma. *Astron. Astrophys.* **193**, 141–147 (1988).
6. Segretain, L. et al. Cooling theory of crystallized white dwarfs. *Astrophys. J.* **434**, 641–651 (1994).
7. Althaus, L. G., García-Berro, E., Isern, J., Córsico, A. H. & Miller Bertolami, M. M. New phase diagrams for dense carbon-oxygen mixtures and white dwarf evolution. *Astron. Astrophys.* **537**, A33 (2012).
8. Horowitz, C. J., Schneider, A. S. & Berry, D. K. Crystallization of carbon–oxygen mixtures in white dwarf stars. *Phys. Rev. Lett.* **104**, 231101 (2010).
9. Hughto, J. et al. Direct molecular dynamics simulation of liquid-solid phase equilibria for a three-component plasma. *Phys. Rev. E* **86**, 066413 (2012).
10. Winget, D. E., et al. An independent method for determining the age of the universe. *Astrophys. J.* **315**, 77–81 (1987).
11. Fontaine, G., Brassard, P. & Bergerson, P. The potential of white dwarf cosmochronology. *Publ. Astron. Soc. Pacif.* **113**, 409–435 (2001).
12. Obertas, A. et al. The onset of convective coupling and freezing in the white dwarfs of 47 Tucanae. *Mon. Not. R. Astron. Soc.* **474**, 677–682 (2018).
13. García-Berro, E. et al. A white dwarf cooling age of 8 Gyr for NGC 6791 from physical separation processes. *Nature* **465**, 194–196 (2010).
14. Bédard, A., Bergeron, P. & Fontaine, G. Measurements of physical parameters of white dwarfs: a test of the mass-radius relation. *Astrophys. J.* **848**, 11 (2017).
15. Gaia Collaboration. Gaia Data Release 2: observational Hertzsprung–Russell diagrams. *Astron. Astrophys.* **616**, A10 (2018).
16. Hansen, B. M. S. et al. The white dwarf cooling sequence of the globular cluster Messier 4. *Astrophys. J.* **574**, L155–L158 (2002).
17. Tremblay, P.-E., Kalirai, J. S., Soderblom, D. R., Cignoni, M. & Cummings, J. White dwarf cosmochronology in the solar neighborhood. *Astrophys. J.* **791**, 92 (2014).
18. Gentile Fusillo, N. P. et al. A Gaia Data Release 2 catalogue of white dwarfs and a comparison with SDSS. *Mon. Not. R. Astron. Soc.* **482**, 4570–4591 (2019).
19. Tremblay, P.-E., Ludwig, H.-G., Steffen, M. & Freytag, B. Spectroscopic analysis of DA white dwarfs with 3D model atmospheres. *Astron. Astrophys.* **559**, A104 (2013).
20. El-Badry, K., Rix, H.-W. & Weisz, D. R. An empirical measurement of the initial–final mass relation with Gaia white dwarfs. *Astrophys. J.* **860**, L17 (2018).
21. Chandrasekhar, S. The highly collapsed configurations of a stellar mass. (Second paper.) *Mon. Not. R. Astron. Soc.* **95**, 207–225 (1935).
22. Kleinman, S. J. et al. SDSS DR7 white dwarf catalog. *Astrophys. J. Suppl. Ser.* **204**, 5 (2013).

23. Bergeron, P., Saffer, R. A. & Liebert, J. A spectroscopic determination of the mass distribution of DA white dwarfs. *Astrophys. J.* **394**, 228–247 (1992).
24. Kalirai, J. S., Richer, H. B., Hansen, B. M. S., Reitzel, D. & Rich, R. M. The dearth of massive, helium-rich white dwarfs in young open star clusters. *Astrophys. J.* **618**, L129–L132 (2005).
25. Tremblay, P.-E. et al. On the evolution of magnetic white dwarfs. *Astrophys. J.* **812**, 19 (2015).
26. Kalirai, J. S. et al. Ultra-deep Hubble Space Telescope imaging of the small Magellanic cloud: the initial mass function of stars with $M \lesssim 1 M_{\odot}$. *Astrophys. J.* **763**, 110 (2013).
27. Bertelli, G., Nasi, E., Girardi, L. & Marigo, P. Scaled solar tracks and isochrones in a large region of the *Z*–*Y* plane. II. From 2.5 to 20 $M_{\odot}$ stars. *Astron. Astrophys.* **508**, 355–369 (2009).
28. Potekhin, A. Y. & Chabrier, G. Equation of state of fully ionized electron–ion plasmas. II. Extension to relativistic densities and to the solid phase. *Phys. Rev. E* **62**, 8554–8563 (2000).
29. Marigo, P. Chemical yields from low- and intermediate-mass stars: model predictions and basic observational constraints. *Astron. Astrophys.* **370**, 194–217 (2001).
30. Mestel, L. & Ruderman, M. A. The energy content of a white dwarf and its rate of cooling. *Mon. Not. R. Astron. Soc.* **136**, 27–38 (1967).

Acknowledgements This research received funding from the European Research Council under the European Union's Horizon 2020 research and innovation programme number 677706 (WD3D) and under the European Union's Seventh Framework Programme (FP/2007- 2013)/ERC Grant Agreement number 320964 (WDTracer). This work made use of data from the European Space Agency (ESA) mission Gaia (https://www.cosmos.esa.int/gaia), processed by the Gaia Data Processing and Analysis Consortium (DPAC, https://www.cosmos.esa.int/web/gaia/dpac/consortium). Funding for the DPAC was provided by national institutions, in particular the institutions participating in the Gaia Multilateral Agreement. Support for J.J.H. was provided by NASA through Hubble Fellowship grant #HST-HF2-51357.001-A, awarded by the Space Telescope Science Institute, which is operated by the Association of Universities for Research in Astronomy, Inc., under NASA contract NAS5-26555.

Author contributions P.-E.T. and B.H.D. identified and characterized the empirical crystallization sequence. G.F. made the evolutionary white-dwarf models used in this work. N.P.G.F., M.A.H. and T.C. constructed the Gaia white-dwarf sample employed in this study and performed the cross-match with other photometric and spectroscopic surveys. P.-E.T., B.T.G., T.R.M., J.J.H. and G.F. wrote the text and developed the argument for a crystallization sequence. E.C. and T.C. characterized the accuracy of Gaia measurements and derived parameters for white dwarfs.

Competing interests The authors declare no competing interests.

Additional information
Reprints and permissions information is available at http://www.nature.com/reprints.
Correspondence and requests for materials should be addressed to P.-E.T.
Publisher's note: Springer Nature remains neutral with regard to jurisdictional claims in published maps and institutional affiliations.